AN ACTIVE MICROVIBRATION ISOLATION SYSTEM

Hirokazu Yoshioka and Nobuyoshi Murai
Takenaka Corporation
1-5-1, Ohtsuka, Inzai, Chiba, 270-1395, Japan

1. INTRODUCTION

With the rapid progress of state-of-the-art R&D technology in the semiconductor and optical instruments industry, as well as other advanced fields such as physics, environmental performance requirement for production facilities and R&D institutes have become increasingly severe. In particular, micro-vibration environments should be maintained at low levels for long periods of time for such high-technology industrial facilities. This need continues to grow. For example, DRAM design rules recently require line widths of only 0.13 μm [1] in the semiconductor industry. The importance of the microvibration control technology is very high for both the equipment and facilities which produce semiconductors. Yang and Agrawal [2] proposed the hybrid base isolation strategy for these kinds of facilities and showed the effectiveness for train induced horizontal vibration.

Vibration isolation tables and floors are widely-applied methods for reducing microvibration of sensitive equipment. For high frequency excitations, use of passive isolation tables using coil springs, air springs or rubber isolators for each piece of equipment are a well-established method. Takahashi et al. [3] developed a 6DOF active microvibration isolation system using voice-coil linear motors and pneumatic actuators that can provide a flexible microvibration environment for high-precision processing and inspection equipment. This system is designed using pseudo absolute displacement and absolute velocity of the table feedback to reduce microvibration of the vibration isolation table in any direction.

Thereafter, a number of active isolation tables, especially for semiconductor manufacturing equipment, have been implemented in practice [4][5][6][7][8]. In these developments, various actuators have been employed (e.g., piezoelectric actuators, electromagnetic actuators and giant magnetostrictive actuators). To reduce the response of the isolation table, various control strategies have been proposed, such as H-infinity control, a combination of feedback and feedforward control, PI control, pole assignment, etc.

In this study, aimed at development of a larger system with a lower profile, we have developed an active microvibration isolation system that takes into account the bending modes of the vibration isolation table in addition to the six rigid body degrees of freedom. To improve the active isolation performance, new controller design using genetic algorithms have been developed. This paper focuses on the process of isolation table development, giving an outline of the system, the control method and the experimental results.

2. OUTLINE OF THE MICROVIBRATION ISOLATION SYSTEM

Fig. 1 gives an outline of the microvibration isolation system. The 2×2 m vibration isolation table indicated by the dashed line in Fig. 1(a) is the object of vibration control. It is supported on air springs (which also serve as pneumatic actuators). This acts as a high-performance passive vibration isolation table. Active control forces are provided to this system through the actuators; a DSP computer calculates the amount of vibration control force required according to the incoming acceleration signals from the sensors.

The profile of the isolation table is restricted to 250 mm so that it can be installed under low-profile grating floors in the clean room of current semiconductor facilities. To meet the requirement and have an isolation table with adequate rigidity, a stiffened plate was employed. The 35 mm steel plate was augmented with 175 mm deep steel members (see hatched region in Fig. 3). The total mass of the table is 1350 kg. Although this isolation table is relatively stiff, its damping is quite low and the bending modes of the vibration isolation table cannot be neglected. The target modes to be controlled in this study are the six rigid body modes and the first six bending modes of the vibration isolation table, as shown in Fig. 2, in the frequency range up to 200 Hz.

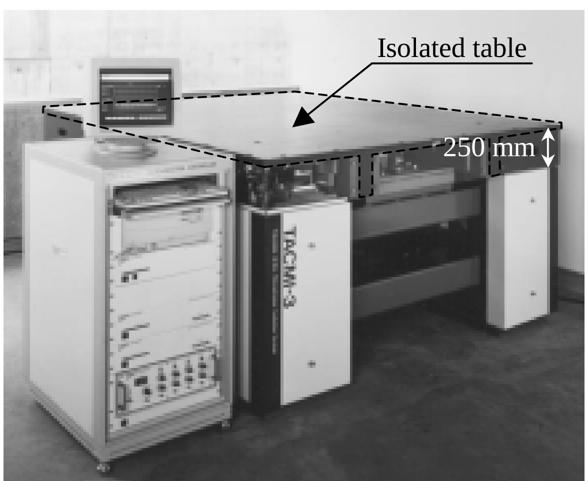

(a) Appearance of the system

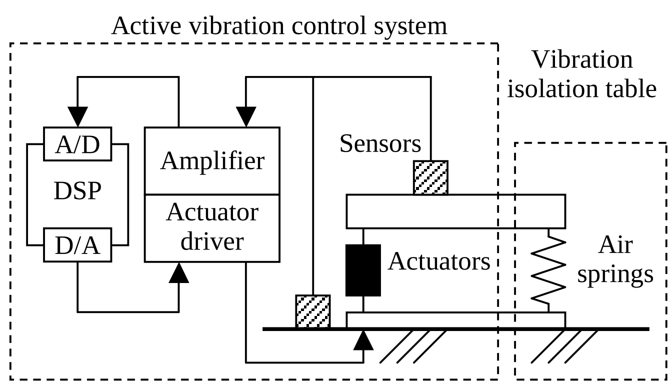

(b) Outline of the system

Fig. 1 Active microvibration isolation table.

Fig. 3 illustrates the layout of the isolation table's actuators and sensors. In this figure, the devices associated with horizontal direction are shown in gray text and symbol. Table 1 gives the characteristics of the actuators, and the types of vibration to be controlled. The pneumatic actuators can generate large control forces, however the response is relatively slow compared to the other actuators. Therefore, pneumatic actuators are only used for control of rigid body vibration in the vertical direction at each of its four corners (i.e., device 1 in Fig. 3). Four voice-coil linear motors (i.e., device 2 in Fig. 3) control the bending modes of the vibration isolation table. Because piezoelectric actuators have a small maximum stroke and fast response time, this actuator is appropriate for control higher mode. In this system, the center of the table is fitted with the piezoelectric actuator (i.e., device 3 in Fig. 3) for the control of the 6th bending mode. Voice-coil linear motors (i.e., device 4 in Fig. 3) are implemented at four locations around the periphery of the table for control of rigid-body vibration in the horizontal direction. A total of seven acceleration sensors (four for vertical measurements and three for lateral, i.e., device 5 in Fig. 3), are installed on the edges and center of the table, with a total of three (one for vertical and two for lateral motions) on the floor.

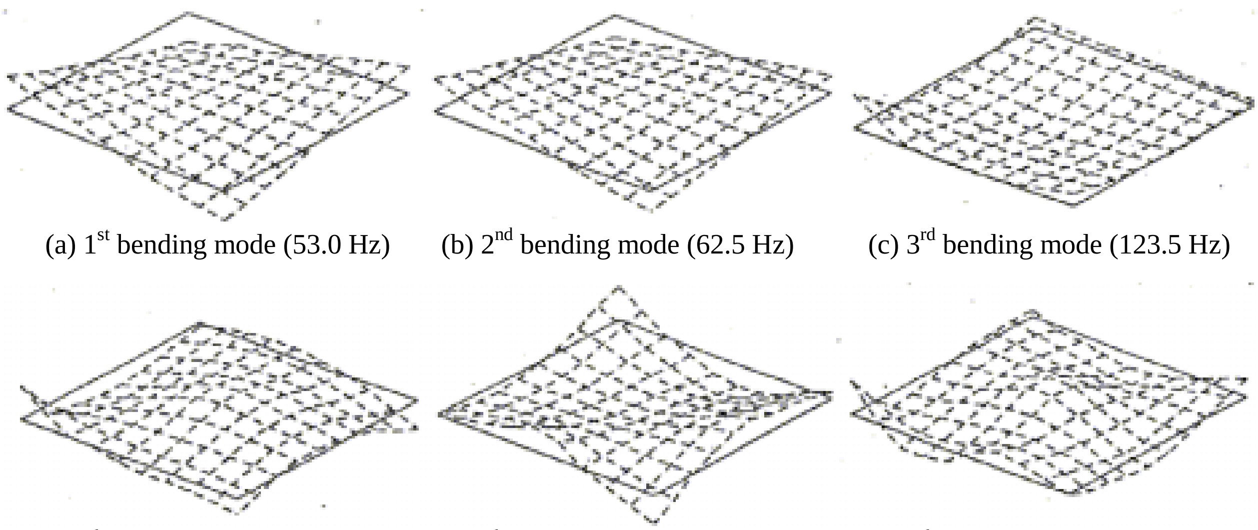

(a) 1st bending mode (53.0 Hz) (b) 2nd bending mode (62.5 Hz) (c) 3rd bending mode (123.5 Hz)

(d) 4th bending mode (153.5 Hz) (b) 5th bending mode (159.9 Hz) (c) 6th bending mode (200.0 Hz)

Fig. 2 Bending modes of the vibration isolation table.

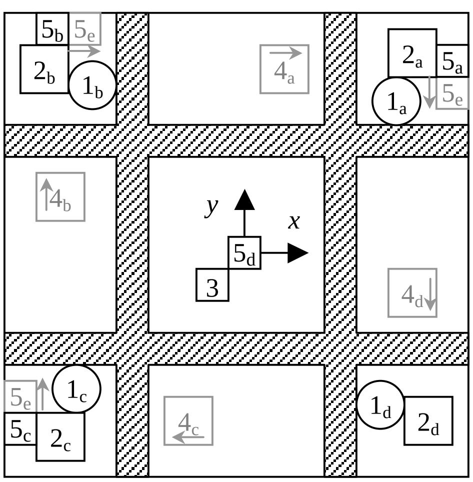

Fig. 3 Layout of actuators and sensors.

1: Pneumatic actuators (vertical)
2: Voice-coil linear motors (vertical)
3: Piezoelectric actuator (vertical)
4: Voice-coil linear motors (horizontal)
5: Acceleration sensors (vertical and horizontal)

Table 1 Characteristics of actuators.

	Maximum force	Stroke (p-p)	Modes to be controlled
Pneumatic actuator	7450N	more than 5mm	Vertical rigid body modes
Voice-coil linear motor	44N	5mm	Bending modes Lateral rigid body modes
Piezoelectric actuator	3430N	75µm	Bending modes

3. MODAL CONTROL LAW USING CLASSICAL FEEDBACK AND FEEDFORWARD METHOD

The equation of motion for the base isolation table corresponding to the relative displacement, **p**, in rectangular coordinates is governed by

$$\mathbf{m}\ddot{\mathbf{p}} + \mathbf{c}\dot{\mathbf{p}} + \mathbf{k}\mathbf{p} = \mathbf{h}_1\ddot{\mathbf{p}}_g + \mathbf{h}_2\mathbf{f} + \mathbf{h}_3\mathbf{u} \tag{1}$$

where **m**, **c** and **k** are the mass, damping and stiffness matrices, respectively. $\mathbf{p}_g$, **f** and **u** are the floor displacement motion vector, other external force vector and the control force vector, respectively. The external force is assumed to be a 3-dimensional floor acceleration and the other forces applied to the isolation table directly.

$$\ddot{\mathbf{p}}_g = \begin{bmatrix} \ddot{x}_g & \ddot{y}_g & \ddot{z}_g \end{bmatrix}^{\mathrm{T}} \text{ and } \mathbf{f} = \begin{bmatrix} f_1 & \cdots & f_m \end{bmatrix}^{\mathrm{T}} \tag{2}$$

The transformation to modal coordinate is given by

$$\mathbf{p} = \mathbf{\Phi}\mathbf{q} \tag{3}$$

where $\mathbf{\Phi}$ is the modal matrix and the modal vector **q**, which includes the 6DOF rigid body modes and n bending modes of the isolation table, can be written as

$$\mathbf{q} = \begin{bmatrix} x & y & z & \theta_x & \theta_y & \theta_z & b_1 & b_2 & \cdots & b_n \end{bmatrix}^{\mathrm{T}} \tag{4}$$

Then, the equation of motion in modal coordinates is given by

$$\mathbf{\Phi}^{\mathrm{T}}\mathbf{m}\mathbf{\Phi}\ddot{\mathbf{q}} + \mathbf{\Phi}^{\mathrm{T}}\mathbf{c}\mathbf{\Phi}\dot{\mathbf{q}} + \mathbf{\Phi}^{\mathrm{T}}\mathbf{k}\mathbf{\Phi}\mathbf{q} = \mathbf{\Phi}^{\mathrm{T}}\mathbf{h}_1\ddot{\mathbf{p}}_g + \mathbf{\Phi}^{\mathrm{T}}\mathbf{h}_2\mathbf{f} + \mathbf{\Phi}^{\mathrm{T}}\mathbf{h}_3\mathbf{u} \tag{5}$$

or

$$\mathbf{M}\ddot{\mathbf{q}} + \mathbf{C}\dot{\mathbf{q}} + \mathbf{K}\mathbf{q} = \mathbf{H}_1\ddot{\mathbf{p}}_g + \mathbf{H}_2\mathbf{f} + \mathbf{H}_3\mathbf{u} \tag{6}$$

where

$$\mathbf{M} = \mathbf{\Phi}^{\mathrm{T}}\mathbf{m}\mathbf{\Phi}, \quad \mathbf{C} = \mathbf{\Phi}^{\mathrm{T}}\mathbf{c}\mathbf{\Phi}, \quad \mathbf{K} = \mathbf{\Phi}^{\mathrm{T}}\mathbf{k}\mathbf{\Phi}, \quad \mathbf{H}_{k=1,3} = \mathbf{\Phi}^{\mathrm{T}}\mathbf{h}_{k=1,3} \tag{7}$$

and **M** and **K** are diagonal matrices. Assuming proportional damping then yields

$$m_i\ddot{q}_i + c_i\dot{q}_i + k_i q_i = \mathbf{h}_{1i}\ddot{\mathbf{p}}_g + \mathbf{h}_{2i}\mathbf{f} + \mathbf{h}_{3i}\mathbf{u} \tag{8}$$

For the translational components, x, y and z, the participation factor associated with the floor excitation are equal to the mass of the corresponding SDOF system. Equation of motion is then written as

$$m_i\ddot{q}_i + c_i\dot{q}_i + k_i q_i = -m_i\ddot{q}_{g\,i} + f_i + u_i \tag{9}$$

where q_{gi}, f_i and u_i are the i^{th} modal floor displacement motion, the other external modal forces and the modal control force, respectively.

The modal control force, u_i, can be determined by many ways. In the case of microvibration control, most of the restrictions on the actuator are insignificant. In this paper, feedback of the absolute velocity response and feedforward of the velocity and displacement of the floor motion are used. Absolute velocity feedback is well known as a classical method [3][9]. This method has the advantage of easy implementation. To improve vibration isolation performance, the feedforward control method is used for the translational rigid body modes. Feedforward control provides an input motion cancellation effect and is capable of cutting off the transmission of vibration from the floor to the vibration isolation table. However, it cannot effectively control external forces imposed directly on the table. Both control forces can be written as

$$u_{i(FB)} = -c_{ai}\dot{q}_i \tag{10}$$

$$u_{i(FF)} = c_{gi}\dot{q}_{gi} + k_{gi}q_{gi} \tag{11}$$

The block diagram of these controllers is shown in Fig. 4. The transfer function to the absolute response for the i^{th} mode becomes

$$\frac{\ddot{q}_i + \ddot{q}_{gi}}{\ddot{q}_{gi}} = \frac{(c_i + c_{gi})s + (k_i + k_{gi})}{m_i s^2 + (c_i + c_{ai})s + k_i} \tag{12}$$

$$\frac{\ddot{q}_i}{f_i} = \frac{1}{m_i s^2 + (c_i + c_{ai})s + k_i} \tag{13}$$

From these equations, it is obvious that the absolute velocity response feedback can change the poles of the transfer functions. This kind of the feedback is especially effective for increasing damping. On the other hand, the ideal feedforward can reduce the response due to floor excitation to zero with coefficients of

$$c_{gi} = -c_i \text{ and } k_{gi} = -k_i \tag{14}$$

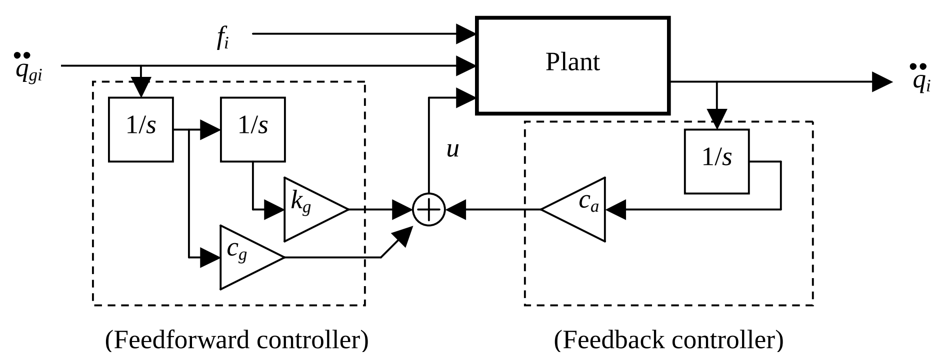

Fig. 4 Block diagram of the classical controller.

Since measuring absolute velocity and displacement directly is difficult, pseudo absolute velocity and displacement is obtained by integration of the measured acceleration signal. An integrator is implemented as $1/(s+a)$, where a is the cutoff frequency of the high-pass filter (HPF), to prevent divergence due to any DC component of the acceleration. Then, the transfer functions with feedback and feedforward controller using pseudo absolute velocity and displacement are

$$\frac{\ddot{q}_i + \ddot{q}_{gi}}{\ddot{q}_{gi}} = \frac{c_i s + k_i + c_{gi} s^2/(s+a) + k_{gi} s^2/(s+a)^2}{m_i s^2 + c_i s + k_i + c_{ai} s^2/(s+a)} \tag{15}$$

$$\frac{\ddot{q}_i}{f_i} = \frac{1}{m_i s^2 + c_i s + k_i + c_{ai} s^2/(s+a)} \tag{16}$$

Fig. 5 shows the typical acceleration transfer function from the floor motion to the modal acceleration response. In this analysis, the horizontal axis is frequency normalized with respect to the natural frequency of the mode. The modal damping is assumed to be 5 %. The cutoff frequency of the HPF is assumed to be 0.1 times to the natural frequency. In the case of absolute velocity feedback, the influence of the high-pass component on the performance is relatively small. The performance with feedforward control becomes worse around the cutoff frequency of the HPF. However feedforward control still has more benefit than only using feedback control.

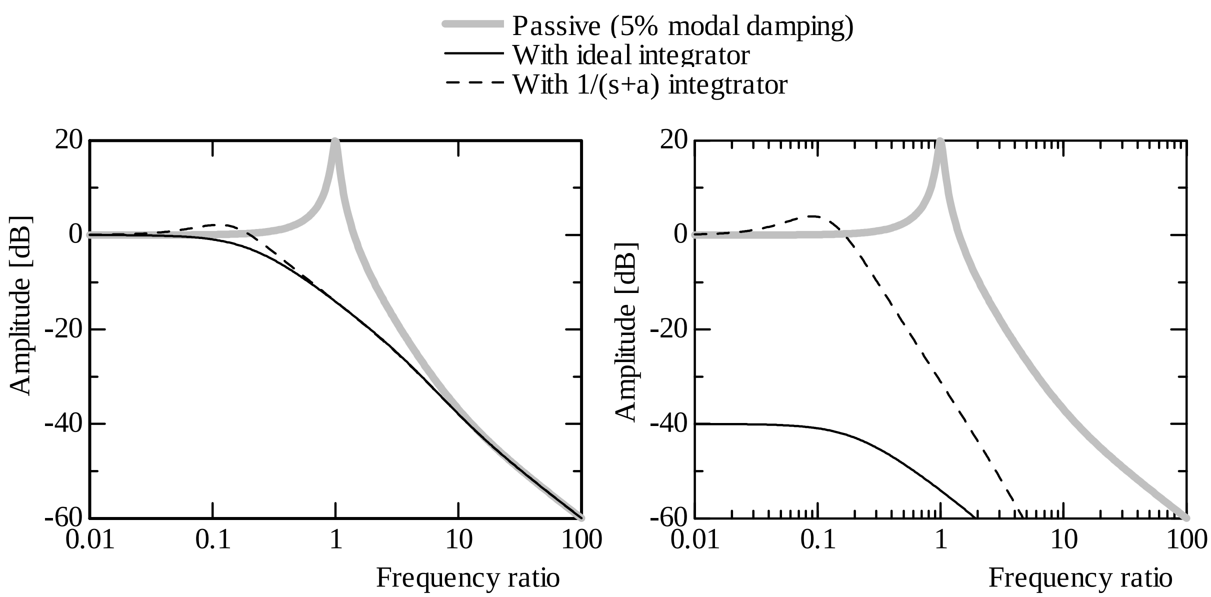

(a) With Feedback control (c_a=c*50)

(b) With feedabck (c_a=50*c) and feedforward (c_{gi}=0.99*c_i, k_{gi}=0.99*k_i)

Fig. 5 Analytical transfer function from ground to the modal acceleration.

For the rocking and the torsional components of the rigid body motion, the participation factor of the floor motion is zero. Therefore, the equation of motion for the i^{th} mode is

$$m_i \ddot{q}_i + c_i \dot{q}_i + k_i q_i = h_{2i} f_i + h_{3i} u_i \tag{17}$$

To control these components, absolute velocity feedback, as expressed in Eq. 10, is used.

As some of the bending modes are not symmetric, such as shown in Fig. 2 (c), the participation factor for the floor excitation is not zero. However, the floor acceleration at high frequencies (over 100 Hz) can be neglected. Therefore, the equation of motion is also expressed as in Eq. 15. The control force for the bending mode, u_{bi}, is given by the following second order filter.

$$m_{bi}\ddot{q}_{bi} + c_{bi}(\dot{q}_{bi} - \dot{q}_i) + k_b(q_{bi} - q_i) = 0 \tag{18}$$

$$u_{bi} = c_{bi}(\dot{q}_{bi} - \dot{q}) + k_{bi}(q_{bi} - q_i) \tag{19}$$

This controller generates a force like that of a tuned mass damper, hence it is termed a virtual tuned mass damper. This type of approach allows the benefits of the TMD, which in general are not applicable to actual isolation systems. In the analysis, modal damping ratio for the bending mode is assumed to be 1%.

In our study, seven acceleration sensors were used to determine the vibration modes of the table for use in the control algorithm. The six rigid body modes and the first bending mode of the isolation table are directly determined based on signals from these seven accelerometers. Contributions from the higher mode's responses are eliminated by low pass filters. For higher bending modes, each mode cannot all be uniquely determined using the available sensors, so those that cannot be separated are eliminated by adjusting the mass and damping of the virtual TMD [10]. Modal testing was conducted to determine the parameters in Eq. 15. Pseudo absolute displacement and velocity are obtained by integrating the accelerations with a time constant of 0.1sec.

4. EXPERIMENTAL RESULTS WITH THE BASIC CONTROLLER

Figs. 6 and 7 show the floor motion and vertical acceleration waveforms at the center of the vibration isolation table during constant microvibration and during an earthquake, respectively. This earthquake occurred at 18:59 on Sept. 6, 1994 with an epicenter in the middle of Ibaraki Prefecture; the measurement point was Inzai-shi, Chiba, JAPAN. Fig. 6 shows that the high-frequency components of microvibration around 0.5 cm/s^2 were eliminated by the passive mode. However, since the low frequency components in the vicinity of the system's natural frequency were enhanced, the overall reduction achieved at the center of the table was about one third of the floor motion. In the active mode, the low-frequency components were eliminated, and the vibration was reduced to about 1/30 at maximum, or about 1/45 in rms terms. The effectiveness of active control in earthquakes of about 8 cm/s^2 was also demonstrated. The maximum vibration reduction achieved was about 1/100, or about 1/60 in rms terms. The maximum acceleration at the center of the table was reduced below 0.1 cm/s^2.

Fig. 8 shows the transmissibility from the floor to the vertical vibration at the center of the vibration isolation table. It is clear that vibration of the table due to floor motion is attenuated at all frequencies. When vibration was controlled by velocity feedback alone, lower frequency vibration, which was enhanced in the passive mode, was reduced. As a result, vibration was damped to below 0 dB over the entire frequency range. In the case of vibrations over 15 Hz, there was no observable difference from the results in passive mode. When the floor motion was fedforward as part of the control, the isolation effect improved by about -10 to -20 dB at frequencies over 2 Hz. Excellent vibration damping effect of -40 dB (1/100) was attained at frequencies over 5 Hz.

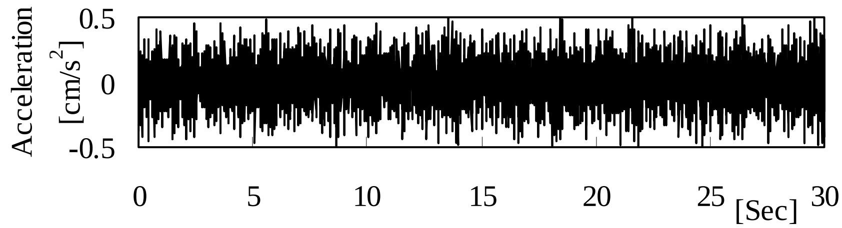

(a) Ground motion (max: 0.550 cm/s^2, rms: 0.186 cm/s^2)

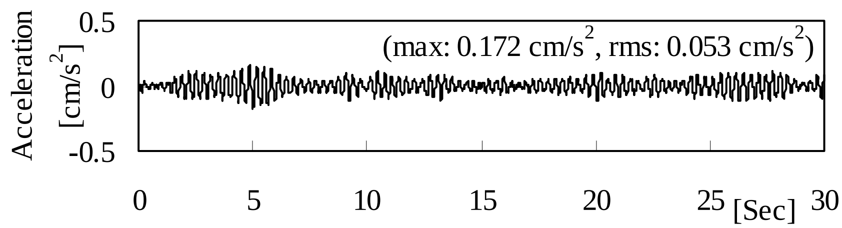

(b) Center of vibration isolation table (passive isolation)

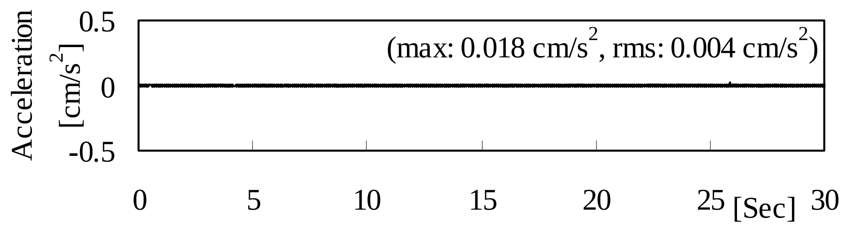

(c) Center of vibration isolation table (active isolation)

Fig. 6 Acceleration in the vertical direction under microvibration.

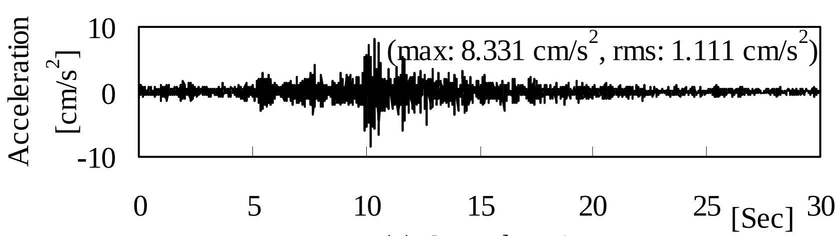

(a) Ground motion

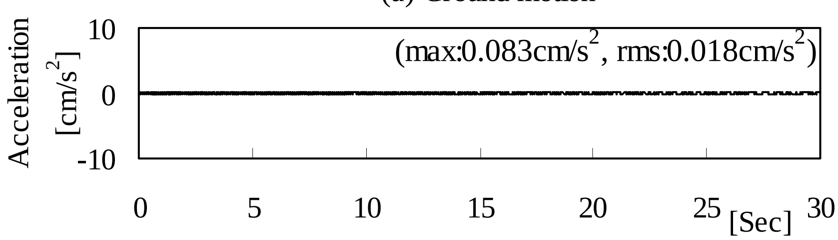

(b) Center of vibration isolation table (active isolation)

Fig. 7 Acceleration in the vertical direction under earthquake.

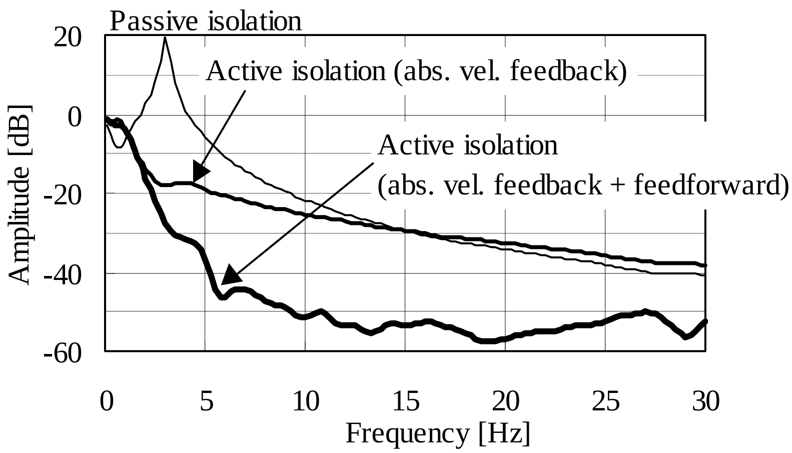

Fig. 8 The effect of adding feedforward control in the vertical direction.

Fig. 9 compares acceleration waveforms for the passive and active modes when an impact excitation was applied to the edge of the vibration isolation table. Fig. 10 shows the resonance amplitude for random excitations applied at the edge of the table. In the passive mode, vibrations continued for over a second after impact excitation. When in the active mode, good vibration damping effects were achieved using the pseudo absolute velocity feedback (*i.e.* sky hook damper) control strategy presented in the previous section. Vibration was damped even within a time scale of around 0.1 sec.

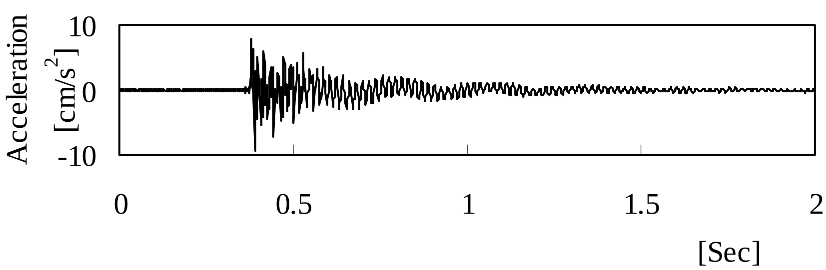

(a) Passive isolation

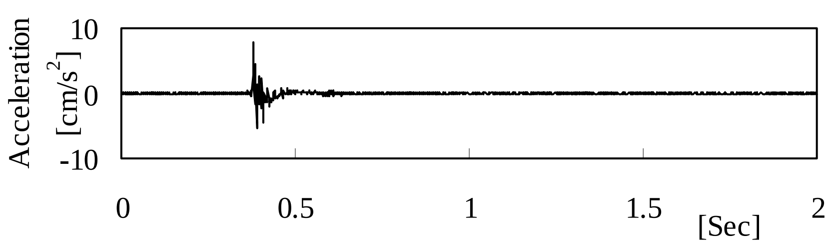

(b) Active isolation

Fig. 9 Acceleration waveform at the vertical sensor 5d
due to vertical impact excitation at edge of vibration isolation table.

The transfer function from the force to the acceleration response of the table was around 25 cm/s^2/N at peak in the passive mode, but this fell to around 4 cm/s^2/N when in the active mode. In some parts of the frequency range, the amplitude in the active mode is greater than that in the passive mode. This is probably due to providing inadequate allowance for the phase lag in the linear motors.

The eccentricity of the mass is not included in the model. However, stability with the mass eccentricity due to a human payload (about 65 kg) was experimentally confirmed.

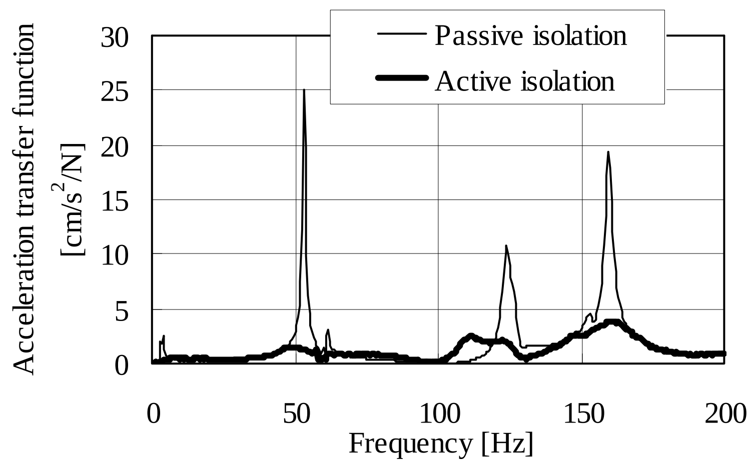

Fig. 10 Transfer function from the force applied at the edge of the isolation table to the acceleration at the vertical sensor 5d.

5. IMPROVEMENT OF THE CONTROL PERFORMANCE USING GENETIC ALGORITHM

The controllers discussed previously do not considered robust stability directly. Therefore feedback control gains were experimentally determined by trial and error. Various methods have been proposed to design optimal robust controllers, such as H-infinity, μ-synthesis and so on. However, most of the existing methods for control design define weighting functions to shape the control loop; they do not specify the transfer function of the closed loop system directly. Therefore trial and error is necessary to obtain the desired transfer function. In the design phase of the microvibration isolation table, the specification is often directly defined by the transfer function. Therefore, a control design algorithm which can directly define the desired transfer function is desirable for this type of problems.

The genetic algorithm [11] has attracted a great deal of attention for its effectiveness for optimization. Some efforrs have been made to employ this idea for controller design [12]. In this study, the desired closed loop transfer function is directly defined, and the desired controller is achieved through use of the genetic algorithm optimization.

The controller can be represented by the product of the biquad filters in the Laplace domain

$$H(s) = \prod_{i=1}^{N} \frac{b_{2i}s^2 + b_{1i}s + b_{0i}}{s^2 + a_{1i}s + a_{0i}} \tag{20}$$

The order of the controller is therefore $2N$.

In the genetic algorithm, each candidate needs to be represented by binary digit associated with genes. Fig. 11 shows the representation of the real number of each coefficient of the filter by the binary digit.

0 or 1	0 or 1	0 or 1	0 or 1	•••	0 or 1	0 or 1	0 or 1	•••	0 or 1
r_1	r_2	r_3	r_4	•••	r_k	R_1	R_2	•••	R_m

Fig. 11 Representation of the real number by the binary digit.

Then each of the coefficients in Equation (20) is represented by a 14-bit floating point number.

$$a_{ij}, b_{ij} = (r_1 \times 2^{-1} + r_2 \times 2^{-2} + \cdots + r_k \times 2^{-k}) \times 2^{(R_1 \times 2^1 + R_2 \times 2^2 + \cdots + R_m \times 2^m)} \quad (21)$$

where k=8 and m=6. Then maximum and minimum values represented by this 14-bit number are about 4.29×10^9 and 2.34×10^{-10}.

The error function to optimize controller for each mode is given by

$$Err = \begin{cases} \infty & if \quad \gamma < W(s) \\ \sqrt{\Sigma |G_d(s) - G_c(s)|^2} & if \quad \gamma \geq W(s) \end{cases} \quad (22)$$

where $G_d(s)$ and $G_c(s)$ are the closed loop transfer function using the desired controller and each candidate, respectively. γ and $W(s)$ are the gain margin of the open loop transfer function and positive-valued weighting function of the gain margin, respectively. Optimization using this error function attempts to make the closed loop transfer function close to a target transfer function without the gain margin dropping below $W(s)$, to ensure robust stability.

A simple genetic algorithm [11] is employed to determine the controller for the each 3 translational rigid body modes. The population is fixed to 30. The rates of crossover and mutation are assumed to be 0.6 and 0.01, respectively. The 4^{th}-order controller, N=2 in Equation (20), is considered. This value is the minimum value which can achieve the desired transfer function. Fig. 12 shows the final acceleration transfer function of the closed loop system from the floor motion to the isolation table in the horizontal (x) direction using the genetic algorithm after the 200^{th} generation. It is clear that the transfer function obtained using the genetic algorithm controller, represented by thick line, is close to the desired controller.

Fig. 13 shows the experimental horizontal (x) modal acceleration transfer function from the floor to the isolation table using the genetic algorithm. Compared with the absolute displacement and velocity feedback with floor motion feedforward, the improved controller using the genetic algorithm can more effectively reduce vibration at low frequencies, particularly around 1 Hz. As a result, vibration reduction performance is more than -20 dB above 1 Hz.

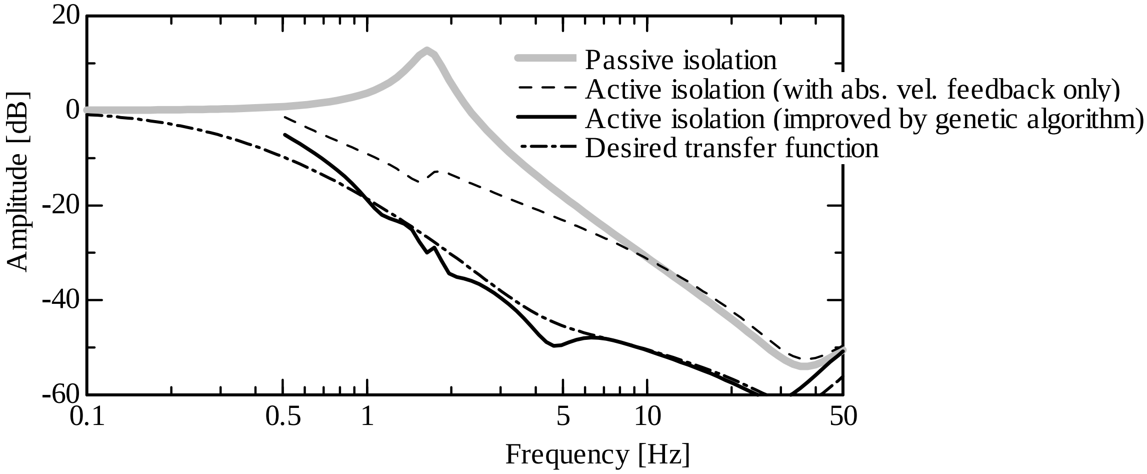

Fig. 12 Analytical horizontal (x) modal acceleration transfer function from the floor to the isolation table.

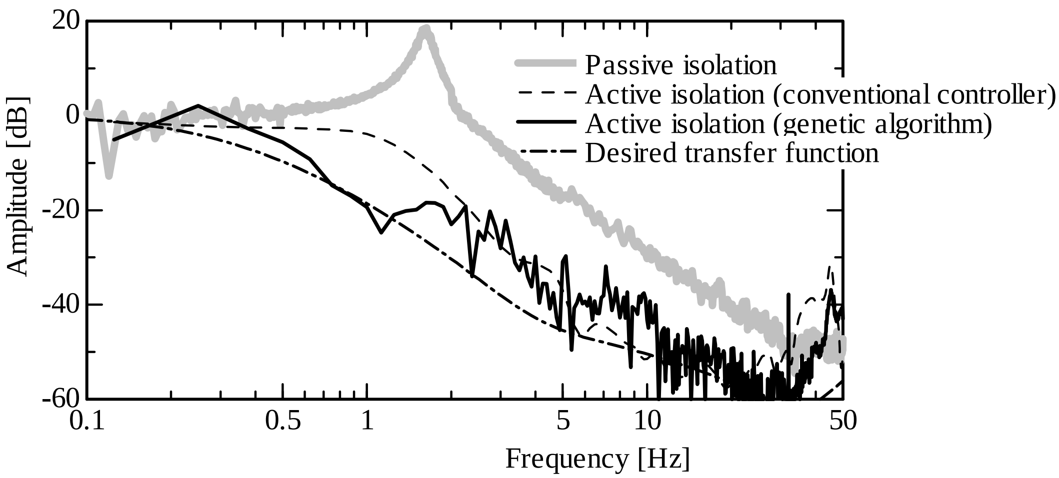

Fig. 13 Experimental horizontal (x) modal acceleration transfer function from the floor to the isolation table.

Fig. 14 shows the 1/3 octave acceleration [1][13] in the vertical direction. The 1/3 octave frequency representation is often used in the microvibration field. The vertical axis corresponds to 1.4 times the RMS of the band-pass filtered acceleration. For floor motion of about 0.5cm/s^2 which is measured at semiconductor facilities, response of the passive isolation table is about 0.1cm/s^2. In the case of active isolation, the acceleration response is less than 0.01cm/s^2 over the entire frequency range. Furthermore, the response with active control is below the generic vibration criterion of vibration sensitive equipment.

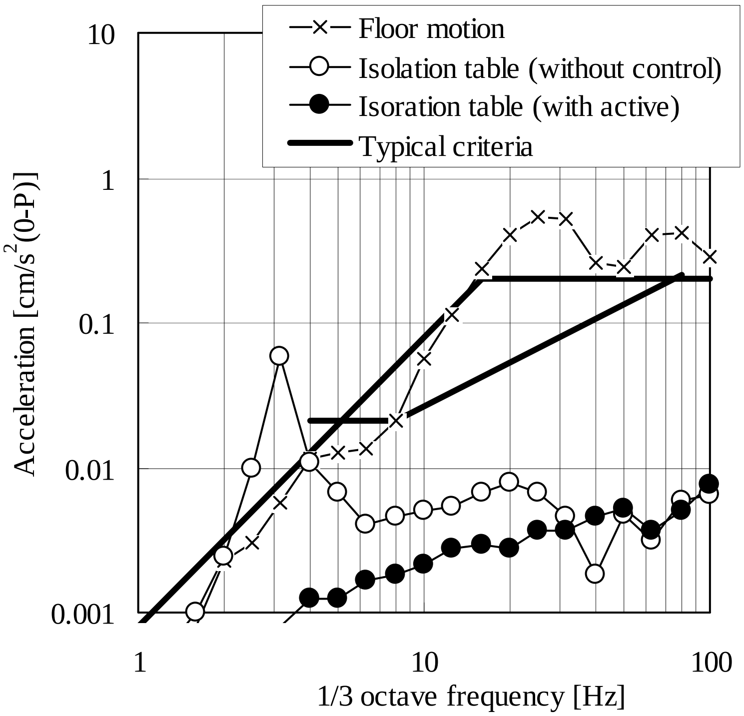

Fig. 14 1/3 octave acceleration in the vertical direction.

6. CONCLUSION

This paper presents an outline of an active vibration control system in which bending modes of the vibration isolation table are taken into account. It is confirmed that using three control methods such as (1) absolute velocity feedback; (2) floor motion feedforward; and (3) virtual TMD method, in combination achieves adequate control of rigid body and bending modes of the table. It is also confirmed that each controller can be improved using genetic algorithm strategies. Excellent vibration isolation performance can be achieved; vibration of the isolation table is reduced to 1/100 of floor motion.

7. ACKNOWLEDGEMENTS

The authors would like to express their great thanks to Tokkyokiki Corporation for producing the prototype active microvibration control system. We also wish to thank Prof. Billie F. Spencer, Jr. of the University of Notre Dame for thorough and helpful advice.

8. REFERENCES

[1] D. Heiland, and K. Beyer, *Vibration in Semiconductor Fabs*, Workshop on Effect of High-Speed Vibration on Structures and Equipment, pp. 63-76, Taiwan, ROC, 1998.

[2] Y.N. Yang and A.K. Agrawal, *Protective System for Microvibration Reduction of Buildings*, Asia-Pacific Workshop on Seismic Design & Retrofit of Structures, pp. 319-333, Aug. 10-12, 1998.

[3] Y. Takahashi, K. Katayama, N. Murai and T. Fujita, *Active Vibration Control System Using Linear Motor*, 5th International Precision Engineering Seminar and Annual Meeting of the Precision Engineering Division, Monterey, California, USA, 1989.

[4] T. Fujita, Y. Tagawa, K. Kajiwara, H. Yoshioka, A. Takeshita and M. Yasuda, *Active 6-DOF Microvibratoin Control System Using Piezoelectric Actuators*, Third International Conference on Adaptive Structures, pp. 514-528, 1992.

[5] T. Fujita, K. Kajiwara, A. Takeshita, H. Yoshioka and M. Yasuda, *Active Microvibration Control System with Elastic Vibration of Equipment-Table System*, 5th International Conference on Adaptive Structures, pp. 612-622, 1994.

[6] K. Watanabe, S. Hara, Y. Kanemitsu, T. Haga, K. Yano, T. Mizuno and R. Katamura, *Combination of* H^{∞} *and PI Control for an Electromagnetically Levitated Vibration Isolation System*, Proceedings of the 35th Conference on Decision and Control, Kobe, Japan, pp. 1223-1228, 1996.

[7] M. Yasuda, T. Osaka and M. Ikeda, *Feedforward Control of a Vibration Isolation System for Disturbance Suppression*, Proceedings of the 35th Conference on Decision and Control, Kobe, Japan, pp. 1229-1233, 1996.

[8] H. Yoshioka and N. Murai, *Active Microvibration Control System by Pole Assignment Method using Genetic Algorithm*, Proc. of the SPIE Conference on Smart Structures and Integrated Systems, Newport Beach, California, pp. 980-986, 1999.

[9] L. Meirovitch and H. Öz, *Active Control of Structures by Modal Synthesis*, in Structural Control, H. H. E. Leipholz (Editor), North-Holland Publishing Co., Amsterdam, pp. 505-521, 1980.

[10] H. Yoshioka, N. Murai, T. Abe and Y. Hashimoto, *Active Microvibration Control System by Considering Elastic Deformation Modes of Vibration Table*, IMAC-XV, JAPAN, 1997.

[11] D.E. Goldberg, *Genetic Algorithms in Search, Optimization & Machine Learning*, Addison-Wesley, 1989.

[12] D. Dasgupta and D.R. McGregor, *Genetically Designing Neuro-controllers for a Dynamic System*, Proceedings of the International Joint Conference on Neural Networks (IJCNN), pp. 2951-2955, Nagoya, Japan, 1993.

[13] E.E. Ungar, D.H. Sturz and C.H. Amick, *Vibration Control Design of High Technology Facilities*, Sound and Vibration, Vol.24, No.7, pp.20-27, 1990.